NOTICE: When government or other drawings, specifications or other data are used for any purpose other than in connection with a definitely related government procurement operation, the U. S. Government thereby incurs no responsibility, nor any obligation whatsoever; and the fact that the Government may have formulated, furnished, or in any way supplied the said drawings, specifications, or other data is not to be regarded by implication or otherwise as in any manner licensing the holder or any other person or corporation, or conveying any rights or permission to manufacture, use or sell any patented invention that may in any way be related thereto.

U. S. Army Ordnance
Ballistics Research Laboratory
Aberdeen Proving Ground, Maryland
Approved Proposal No. 3175
Authorization No. 4086

EXPLOSIVES RESEARCH LABORATORY

150 700

HYPERVELOCITY IMPACT PHENOMENA

Quarterly Report
March 1, 1962 to May 31, 1962

BUREAU OF MINES, PITTSBURGH, PA.

UNITED STATES
DEPARTMENT OF
THE INTERIOR

HYPERVELOCITY IMPACT PHENOMENA

Quarterly Report

March 1, 1962 to May 31, 1962

Prepared for:

U. S. Army Ordnance
Ballistics Research Laboratory
Aberdeen Proving Ground, Maryland
Approved Proposal No. 3175
Authorization No. 4086

by

Karl R. Becker

Richard W. Watson

Frank C. Gibson

Approved by:

Robert W. Van Dolah, Chief
Explosives Research Laboratory

U. S. Department of the Interior
Bureau of Mines
Pittsburgh, Pa.
June 22, 1962

A

HYPERVELOCITY IMPACT PHENOMENA

Introduction

~~The purpose of this investigation is to study~~ the parameters governing the failure of thin metal plates under the impact of high-speed fragments (are being studied); special emphasis is placed on the lightweight structural alloys. The geometrical features of the perforations, together with the spatial, mass, and velocity distributions of the ejecta produced in the perforation process, are (considered) ~~of immediate interest. Since these variables are strongly dependent on the characteristics of the impacting projectile as well as the physical properties of the target material, a variety of experimental approaches to the problem are clearly evident. In an effort to systematize the approach and at the same time gain information that will be of immediate practical value,~~ a few select target materials (e.g., Al and Pb) are currently being investigated under impact conditions that involve the same projectile geometry but different impact velocities.

Behind-Target Effects

Spall Mass Distribution Data

An initial effort toward determining the distribution of spall mass behind thin targets was presented and discussed in the preceding report[1/]. The investigation involved 3.17 km/sec. (23.5 mg.) steel projectiles impacting various thicknesses of 2024-T3 aluminum at normal incidence. Distribution plots for the combined projectile and target

---

1/ Becker, K. R., Watson, R. W., and Gibson, F. C., Hypervelocity Impact Phenomena: Bureau of Mines, April 5, 1962.

masses, as well as for the target mass alone, were presented. One pertinent result obtained was that the distribution curves were qualitatively similar to those obtained for the population (number of spall particles) distribution. Additional data for 4.0 km/sec. projectiles are now available; the new data is presented and compared with the initial data.

The new data involves studies on three thicknesses (1/16, 2/16, and 3/16 inches) of 2024-T3 aluminum targets impacted by 4.0 km/sec. projectiles at normal incidence. The spall products were collected in gelatin and separated into six ring elements by means of a technique described in the previous report. The spall products from each ring element were further separated, by chemical analysis, into either target spall (aluminum fragments) or projectile particles (steel fragments). The spall distribution curves are presented in Figures 1, 2, and 3; the figures show the spall distributions for the combined target-projectile spall system and for the target and projectile spall separately. Tabulations of data associated with the plots are given in Tables I and II. The plots show $\frac{\Delta M}{\Delta \Omega}$ vs $\frac{\theta}{2}$ where Δ M is the mass of spall in a given ring element, $\Delta \Omega$ is the corresponding subtended element of solid angle and $\frac{\theta}{2}$ is a radially sensitive coordinate defined in Figure 4. Each figure contains three curves where each curve represents a target thickness. One qualitative characteristic of all the curves is similar - mass density decreases monotonically with increasing values of $\frac{\theta}{2}$, hence the spall mass is most dense directly

beneath the perforation in the target and diminishes radially outward. Also evident is the target thickness effect; an increase in target thickness results in an increase in total recovered spall mass and results in greater mass densities $\left(\frac{\Delta M}{\Delta \Omega}\right)$ at given values of $\frac{\theta}{2}$.

It is interesting to note that the correlation between target thickness and recovered mass applies to not only the target material but also to the recovered projectile material (see Figure 3). Total recovered projectile masses for different target thicknesses are tabulated on the figure and show that total recovered projectile masses for 1/16, 2/16, and 3/16-inch thick targets are respectively 6.1, 10.1, and 15.9 milligrams (the original projectile mass was about 23.5 milligrams). Thus, one is able to recover larger amounts of projectile material through increasingly thicker targets; there seems little doubt but that this is the case since the data are quite reproducible. (It might be remembered that for lower projectile velocities, the amount of projectile material projected through the target was independent of the target thickness so long as the target thickness is well below the maximum crater depth.) The dependence of transmitted projectile material upon target thickness cannot be satisfactorily explained without a detailed knowledge of the shock interactions taking place within the target. An attempt to gain some knowledge in this area is contemplated and is quite likely to produce information that would be useful in resolving experimental observations of spall phenomena.

The 4.0 km/sec. spall mass distribution data can be compared with results previously obtained from 3.17 km/sec. projectiles. This is accomplished by reducing the data by the normalizing factor $\frac{1}{M_i}$ where M_i is the total mass of the spall fragments for a given velocity-thickness set of data. The comparison is made on Figure 5 and shows $\frac{1}{M_i} \frac{\Delta M_i}{\Delta \Omega}$ vs $\frac{\theta}{2}$ at two impact velocities for both the projectile and target spall masses. The plot illustrates two interesting characteristics of spall phenomena: (1) the percentage of either target spall mass or projectile spall mass, found in any given element of space behind the target is relatively insensitive to the impact velocity; (2) there is a difference in the distribution of the target spall mass and projectile spall mass - the projectile spall mass is not dispersed as much in a radial direction.

Spall Population Distribution Data

In view of the fact that the total spall mass has been separated into projectile mass and target mass and treated individually, it seemed desirable to apply the same treatment to the population distribution of each type of spall particle.

Previous data, obtained by a relatively simple technique, did not distinguish the number of projectile particles from target spall particles. A limited amount of data, employing a somewhat more time consuming technique which does allow the desired distinction, are now available. The technique is, up to a point, identical to that used for mass distribution determinations: the spall particles are collected in

gelatin; the gelatin is separated into ring elements and each gelatin ring element is dissolved in hot water; the spall particles are filtered out, dried and counted. At this point the steel projectile particles are separated from the aluminum target particles by repeated passes of a magnet beneath the paper containing the mixture of spall particles and the separated aluminum particles are counted again. The projectile particles were not counted because the magnetized steel particles were attracted to each other; the number of projectile particles was the difference between the first two counts described above.

The extent of data obtained by this technique amounts to 12 shots (3 shots each for two target thicknesses and two projectile velocities). The targets used were 2/16 and 3/16-inch thick 2024-T3 aluminum. They were impacted by both 3.17 km/sec. and 4.0 km/sec. projectiles at normal incidence. The treated data are plotted on Figure 6 and tabulated in Table III. The plot shows $\frac{1}{N_i} \frac{\Delta N_i}{\Delta \Omega}$ as a function of $\frac{\theta}{2}$ and gives data points for both types of spall material at two impact velocities; the results have been averaged for the two target thicknesses. This plot allows one to compare the relative percentage of the total number of projectile (steel) particles found in a given $\frac{\theta}{2}$ element with the relative percentage of the total number of target (aluminum) particles found in the same $\frac{\theta}{2}$ element. Since the plotted data points seem to define two different curves each characterized by particle type rather than by impact velocity, the following conclusions are made:

(1) both the projectile and target spall population distributions are relatively independent of impact velocity; (2) the projectile particles are not distributed in the same manner as the target spall particles; the projectile spall particles have a tendency to be grouped more closely about $\frac{\theta}{2} = 0$.

The conclusions arrived at for the population distributions are similar to those pertaining to the mass distribution data; the correlation between number and mass is simply an indication that the distribution of particle size is not particularly dependent upon $\frac{\theta}{2}$.

One other useful bit of information is available from these data; for a given impact situation, about 62% of the spall fragments are target spall fragments and 38% are projectile fragments (see Table III for a tabulation of this comparison for each velocity-thickness group).

Individual Spall Particle Mass and Size

Sufficient data associated with aggregate numbers and masses of spall particles are now available, under varying experimental conditions, so that rough indications of average individual particle mass and size are possible.

A plot illustrating the dependency of average individual particle mass as a function of target thickness for the parameters - impact velocity and spall particle type is presented in Figure 7. The effect shown is an average over all the space increments. The data for 1/16 inch target thickness is an average for both projectile and target spall

particles because no data relating to a separation of the two types of particles are available. Several characteristics of the data are worthy of note: (1) for given target thickness, the average mass of both the projectile particles and target particles is relatively insensitive to impact velocity; (2) the average mass of both target and projectile particles increases substantially with increases in the target thickness; the ratio between masses for 3/16-inch thick targets as compared to 1/16 inch targets is about an order of magnitude; (3) the average mass of target spall particles is roughly 2 to 3 times that of the projectile spall particles at the two thicknesses where such a comparison is possible. Since the ratio of the density of steel to that of aluminum is about 3, the relative volume of an average individual target spall particle is about 6 to 9 times that of an average individual projectile particle.

Spall Population Distributions for Oblique Impacts

Distributions associated with oblique impacts are not complete, however, certain interesting observations pertaining to the center of spall populations are evident. Oblique impact studies involved three impact angles - α = 50 degrees, α = 60 degrees, and α = 70 degrees; the target material was aluminum 2024-T3 in thickness sizes ranging from 1/32 inch up to 1/8 inch. All targets were impacted by 4.0 km/sec., 23.5 mg., steel projectiles. Three shots were made for each thickness-impact angle combination. The population of spall particles was deter-

mined by counting holes in 1 mil thick aluminum witness targets located 6-1/2 inches beneath the target plates. In addition, another count was taken of the number of particles that were capable of penetrating an additional 7 mils of aluminum foil. The centers of population were determined by considering the position of the holes relative to the origin. Thus, it is possible to find the centers of populations and distributions for essentially all the spall fragments and also for those penetrating the back-up target. A tabulation of the centers of population is given in Table IV; the corresponding plot is Figure 8 which gives the displacement angle $(\frac{\theta}{2})$ as a function of impact angle (α) with target thickness as a parameter. The displacement angle is a measure of the displacement of the center of spall population relative to point 0 on Figure 4. The plot also shows separate data points for the spall particles having higher penetration capabilities; these are identified in the key under the heading - "10%" because in each case, about 10% of the total number of spall particles were capable of penetrating the back-up target regardless of the target thickness or impact angle. Significant features of the plot are as follows: (1) the data are best represented by four curves, each defining a different target thickness group; and increase in target thickness results in a decrease in displacement angle at given impact angle value; (2) although the ten percentile groups appear to yield slightly lower displacement angles than corresponding 100 percentile groups, the difference in most cases is not particularly significant and it is concluded that they are not

different; (3) for given target thickness, displacement angle reaches a maximum at an impact angle of about 50 to 60 degrees; further increases in impact angle appear to result in a decrease in displacement angle. It should be mentioned, however, that the form of $\frac{\theta}{2}$ vs α curves is somewhat distorted here if one considers the increased thickness due to obliquity to be important because then the effective target thickness would increase with the angle of impact and the curves shown on the plot would not represent a constant thickness. In any event, an attempt to apply corrections to the $\frac{\theta}{2}$ values in order to account for the differences in effective thicknesses, did not alter the qualitative characteristics of the $\frac{\theta}{2}$ vs α curves; (4) the displacement angle is substantially less than the impact angle, e.g., at an impact angle of 60 degress, displacement angles of about 40, 32, 27, and 17 degrees for respective target thicknesses of 1/32, 1/16, 3/32, and 1/8 inches are obtained; (5) further work on the oblique impact data is contemplated; it remains to find the distributions about the center of impact on either the witness plane or perhaps on a plane perpendicular to the displacement vector.

Summary of Behind-Target Effects

(1) When the spall mass is separated into target spall mass and projectile spall masses, it is found that the masses of both types of spall are symmetrically distributed about the center of impact; however, the projectile material is more closely grouped about the center

of impact. The distributions of each type of spall are, however, independent of impact velocity.

(2) The same conclusions given in (1) for the spall mass apply to the spall populations (numbers of spall particles). Roughly 62% of the total number of spall particles is target material; the balance is projectile material.

(3) The average mass of a spall particle (projectile particle or target particle) depends markedly upon the target thickness and is relatively independent of impact velocity. When the target thickness is increased from 1/16 inch to 3/16 inch, the average mass of target spall particles increases by roughly an order of magnitude. At given target thickness, the target particles are 2 to 3 times as heavy as the projectiles; due to the difference in densities the volume of an average target particle is roughly 7 times that of its steel counterpart.

(4) For targets impacted at oblique angles, the displacement of the center of spall impact is in the direction of the projectile travel; however, the angle of displacement is always less than the angle of impact. The angle of displacement is dependent upon both the angle of impact and the target thickness; for given angle of impact, increasing target thickness corresponds to decreasing displacement angle. For given target thickness, the displacement angle maximizes at impact angles of from 50 degrees to 60 degrees.

Two other interesting results were obtained from oblique impact studies: (1) the percentage of spall fragments having superior pene-

tration capabilities is independent of target thickness or impact angle; (2) displacement angles, obtained from the spall patterns of the "superior" spall particles, are not substantially different from those obtained for the complete spall pattern containing spall particles of lower penetration capabilities.

Ballistic Impulse Studies

The experimental program to determine the manner in which the incident projectile momentum is partitioned between target impulse and the momentum of the material ejected from the target was continued. Previously reported studies using aluminum targets impacted by 0.0234 gram steel projectiles having an initial velocity of 3.17 km/sec. have been extended to cover impacts at 4 km/sec. In addition, the preliminary study with lead targets carried out at 3.17 km/sec. has been extended to include impacts at 4.0 km/sec. and 5.0 km/sec.

Studies with 2024-T3 Aluminum

Target impulse as a function of target thickness was measured for 1/16", 2/16", 3/16", 4/16", 5/16" and 3/4" thick 2024-T3 aluminum targets impacted with steel cylinders having an initial mass of 0.0234 grams and a velocity of 4.0 km/sec. With the exception of one minor change the pendulum arrangement described in the last report was used for this purpose - the carbon paper sheet used for recording pendulum deflection in the 3.17 km/sec. impact experiments was replaced by a lightly smoked-glass plate for the 4 km/sec. studies. This was done

in a reasonably successful effort to further reduce the friction of the recording system. The results of this series of tests are presented in Table V and are compared with the results obtained in the 3.17 km/sec. studies in Figure 9.

A consideration of the results obtained at 4.0 km/sec. indicates that the same behavior noted at 3.17 km/sec. studies is exhibited at 4.0 km/sec., that is, the impacts can be considered as being essentially inelastic where only the momentum of the incident projectile is transferred to the target-spall system. It should be pointed out that the evidence for this observation is not quite as strong as that presented for the series of tests carried out at 3.17 km/sec. This is partly due to the fact that while the velocity of the 4.0 km/sec. projectiles is accurately known the delivered mass has not been precisely determined to date. The experimental difficulties associated with this measurement were noted earlier in this report. However, average recovered masses as high as 15.9 milligrams have been reported. On the assumption of inelastic impact, the average forward momentum obtained for "semi-infinite" impacts at 4.0 km/sec. leads to a value of 21.4 milligrams for delivered mass. In view of the similarity between the results obtained with exposed "semi-infinite" targets and those faced with fiberboard - a combination that produces little front surface ejecta - the latter value of delivered mass can be considered to be a reasonable estimate.

Another observation used to support the inelastic collision model proposed for the tests at 3.17 km/sec. was the fact that in this case the difference between the mass lost by the target and the mass of target material recovered in the behind-target studies was small, demonstrating that little material was ejected from the front surface of the target. This is not the case for impacts at 4.0 km/sec. Careful mass lost and mass recovered measurements indicate that a considerable percentage of the mass lost by thin targets impacted at 4.0 km/sec. is lost from the front surface of the targets. This is illustrated in Figure 10 where the percentage mass lost from the first surface of thin targets are compared for impacts at 3.17 km/sec. and 4.0 km/sec. If these results are to be reconciled with the results of the impulse studies one must conclude that the velocity associated with the material ejected from the front surface of thin aluminum targets is very low over the impact velocity range investigated.

Studies with Lead Targets

Unlike aluminum impacts, where only the projectile momentum is transferred to the target-spall system, initial tests with lead at 3.17 km/sec. clearly demonstrated the phenomena of momentum multiplication.[1/] Since this effect is of prime importance in protection design considerations, work with lead targets has continued. The initial target impulse studies carried out at 3.17 km/sec. with relatively thick targets have been extended to include targets having thicknesses of 1/16",

2/16", and 3/16". These results are presented in Table VI.

As a result of the momentum associated with the material ejected from the front surface of the targets these data are inadequate for determining the values of spall momentum for the various thicknesses tested. In order to evaluate this parameter an additional series of tests was conducted in which total forward momentum was measured for targets of different thicknesses. The details of the target arrangement used in this series of tests are shown in Figure 11. The results of these tests, also presented in Table VI, coupled with the target impulse measurements were used to calculate the values of spall momentum associated with each target thickness. The overall test results are shown in Figure 12.

Perhaps the most significant feature of this series of experiments is the fact that the total forward momentum imparted to the target-spall system is essentially independent of target thickness for thicknesses 1/16 inch or greater. This is clearly illustrated in Figure 13 where the measured values of total forward momentum are plotted against target thickness. The 1/16 inch thickness corresponds very closely to the primary penetration expected for these projectiles on the basis of hydrodynamic consideration*.

The purpose of another lead-target investigation was to determine the behavior of the ratio $\frac{i}{\mu}$ as a function of impact velocity. It will

---

* From the hydrodynamic penetration formula, $P = \ell_f \sqrt{\rho_f / \rho_t}$, a 1/16 inch long steel projectile would penetrate to a depth of 0.052 inches in a lead target before expending itself.

be recalled that on the basis of Bryan's treatment of oblique impact this parameter should be independent of impact velocity[1]. Measurements carried out at 3.17 km/sec., 4.0 km/sec., and 5.0 km/sec. indicate that $\frac{i_n}{\mu}$ monotonically decreases over the range investigated.

The standard projectors developed at this laboratory were used for the tests at 3.17 km/sec. and 4.0 km/sec.; for the tests at 5.0 km/sec. an air-cavity projection system developed at B.R.L. was used. Extensive calibrations of this projector system showed that it consistently delivered a mass of 0.18 $\pm$ .013 grams at a velocity of 5.0 $\pm$ .095 km/sec. The projectile material is steel as in the case of the standard projectors used here. The shape of the projectile, however, cannot be accurately controlled. This would lead to differences in crater profile with some target materials, depending on the attitude of the projectile at impact. Since craters in lead, produced by these projectiles are essentially hemispherical this consideration is of no importance in this discussion.

The results of this series of tests are tabulated in Table VII and illustrated in Figure 14 where i_n, μ, and the ratio $\frac{i_n}{\mu}$ are plotted as functions of impact velocity. It will be noted that i_n shows a tendency to increase with impact velocity. However, the normalized mass lost is a much more rapidly increasing function of impact velocity and as a consequence the ratio of the normalized momentum to the normalized mass is a uniformly decreasing function of impact velocity. This observation has no simple interpretation in terms of Bryan's theoretical treatment.

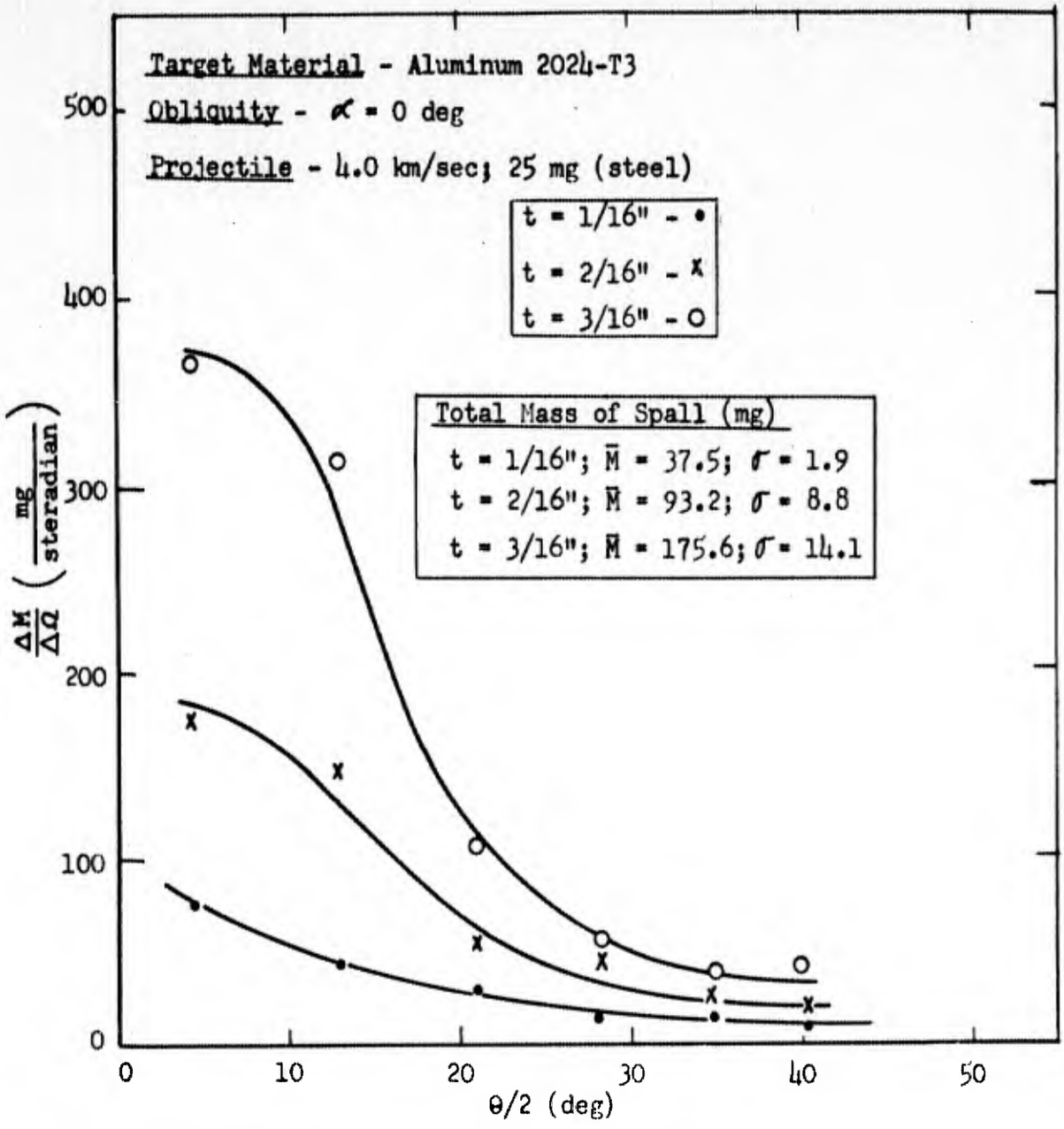

Fig. 1 Plot illustrating the mass distribution of spall (projectile and target spall) behind thin targets for three thicknesses of Aluminum 2024-T3. The targets were impacted by 4.0 km/sec, steel, projectiles at normal incidence. The plot gives mass "density" as a function of one half the dispersion angle.

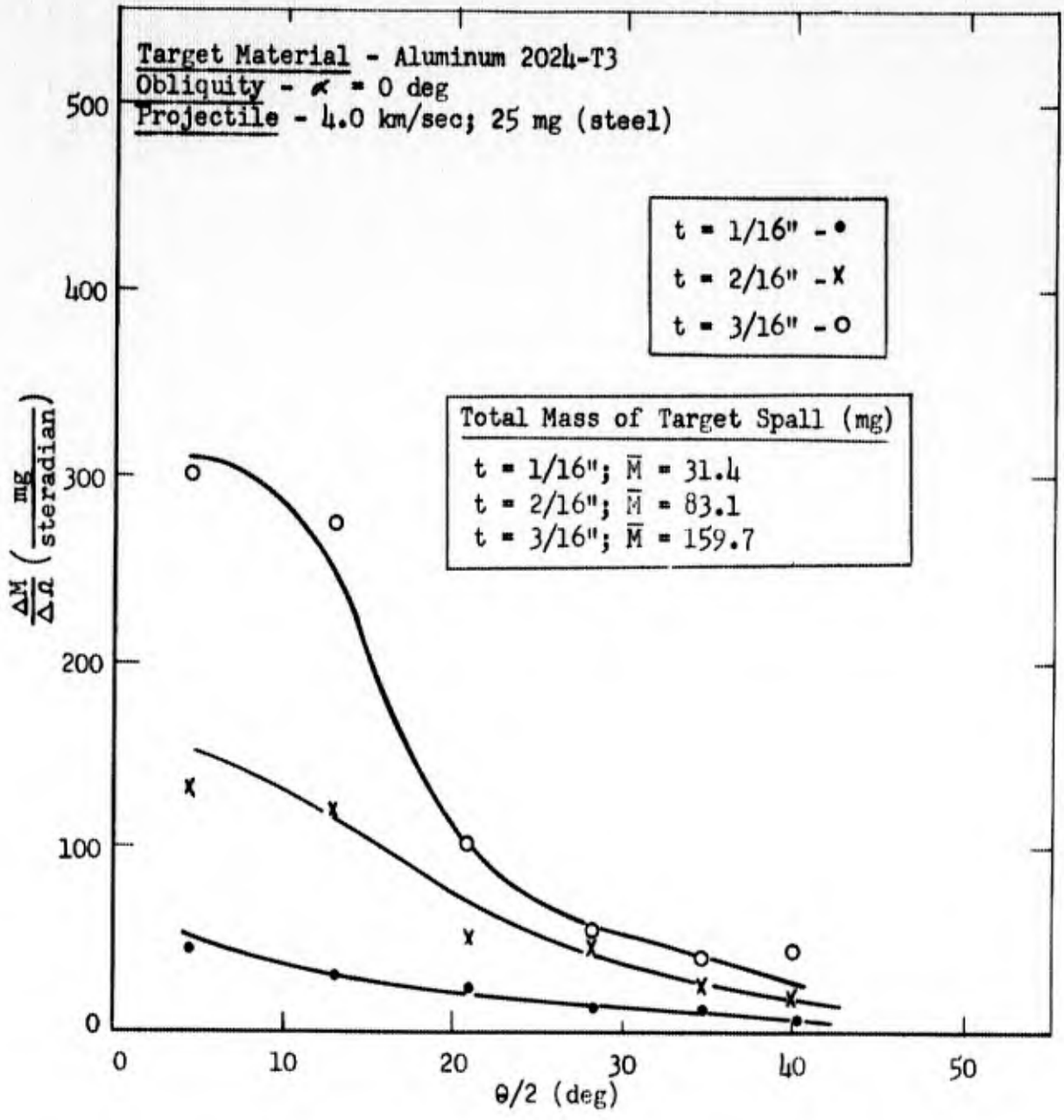

Fig. 2 Plot illustrating the mass distribution of spall (target spall only) behind thin targets for a situation where 4.0 km/sec steel, projectiles impacted Al. 2024-T3 targets at normal incidence. The plot shows mass "density" as a function of one half the dispersion angle.

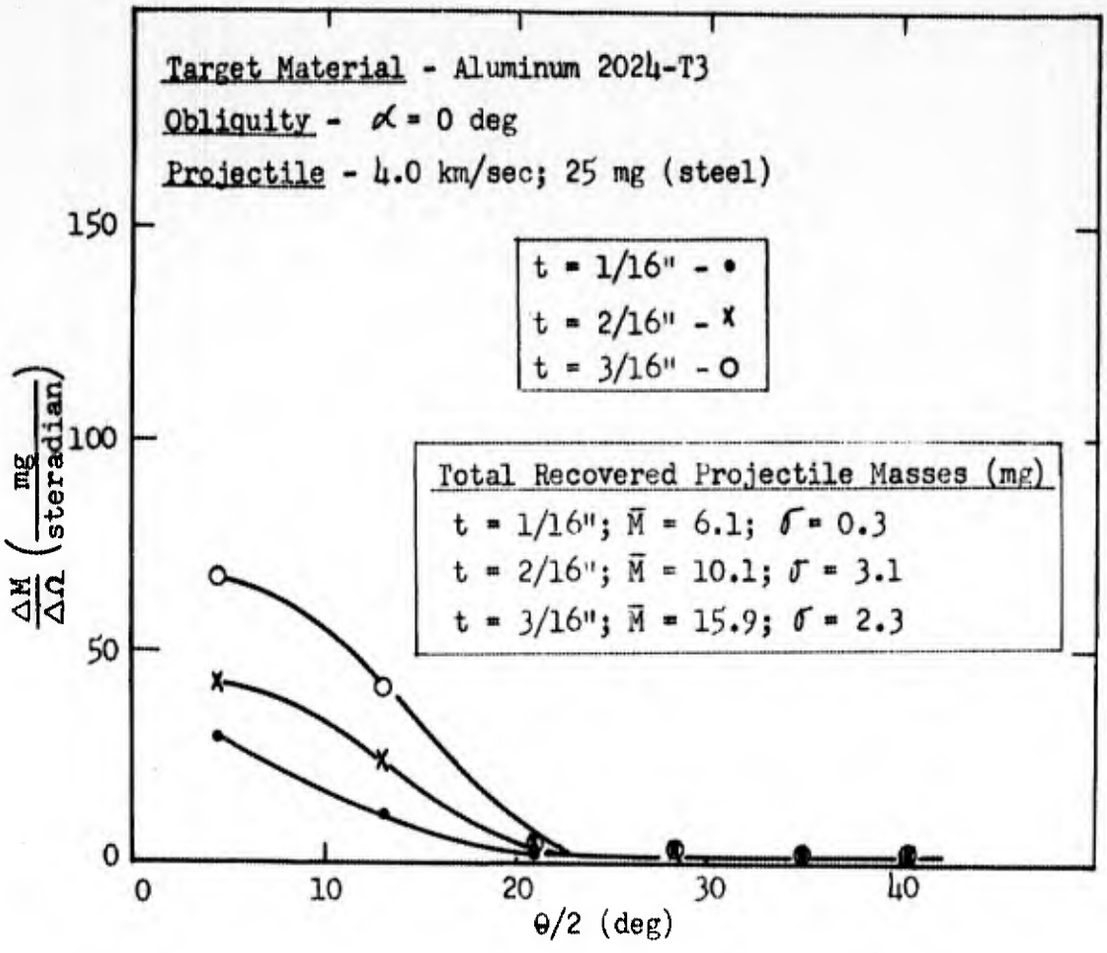

Fig. 3 Plot illustrating the mass distribution of projectile fragments behind thin Aluminum 2024-T3 targets impacted by 4.0 km/sec; 25 mg, steel projectiles at normal incidence. The plot gives mass "density" as a function of one half the dispersion angle.

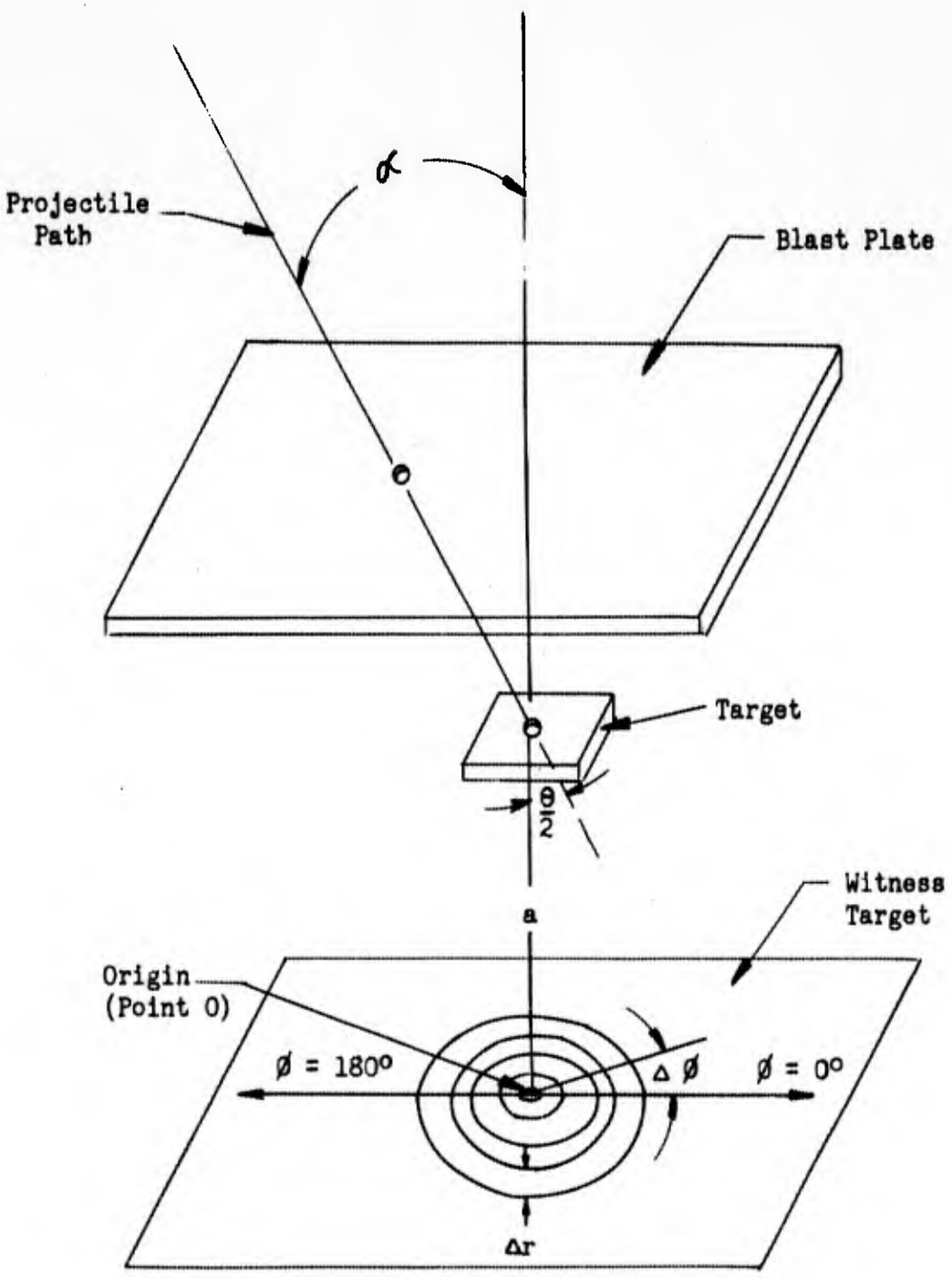

Fig. 4 Sketch illustrating geometric details of the experimental set-up for determining the spatial distribution of spall fragments.

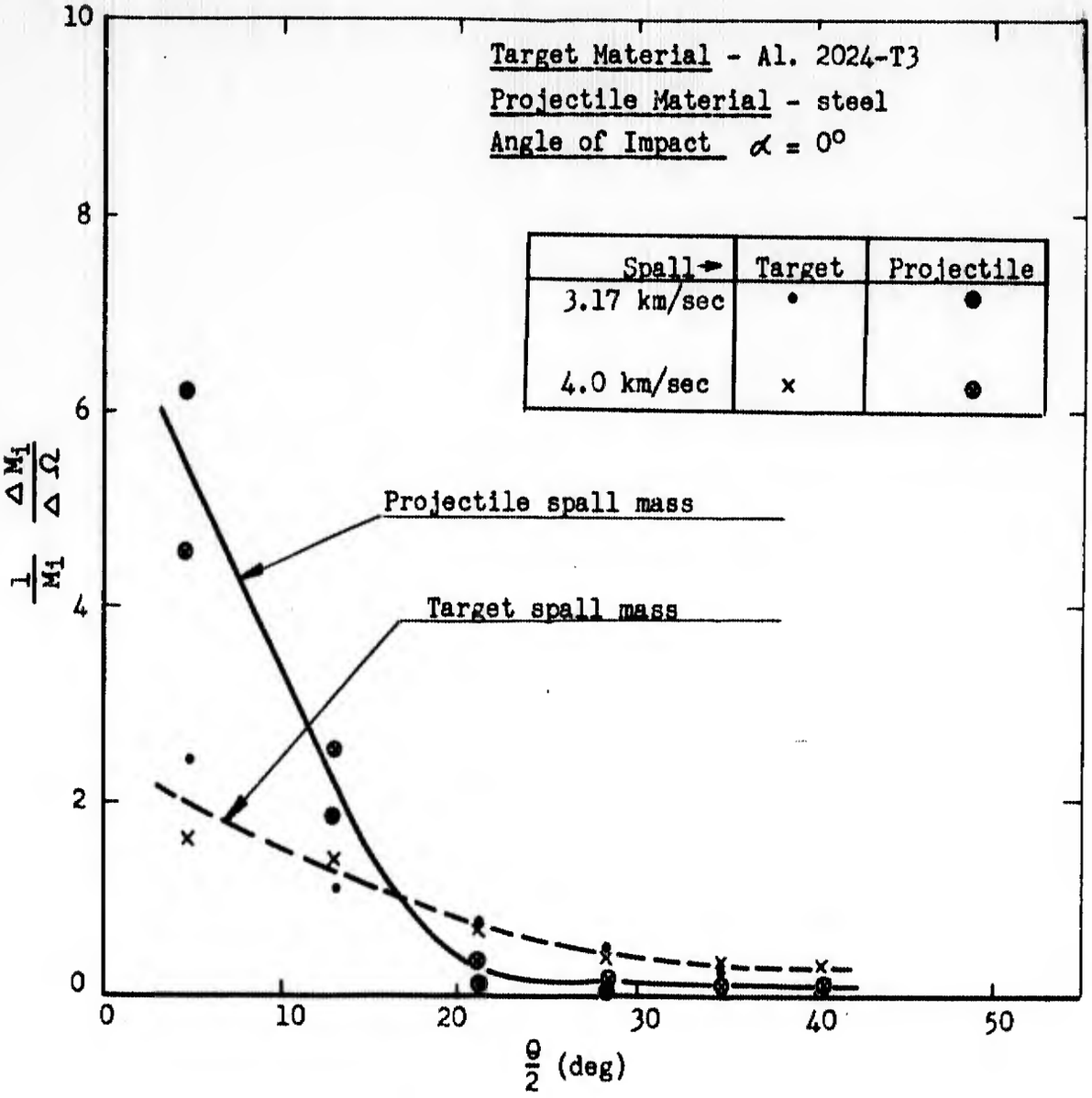

Fig. 5 Plot of normalized mass distribution data as a function of $\theta/2$ for both the projectile spall mass and target spall mass at two impact velocities.

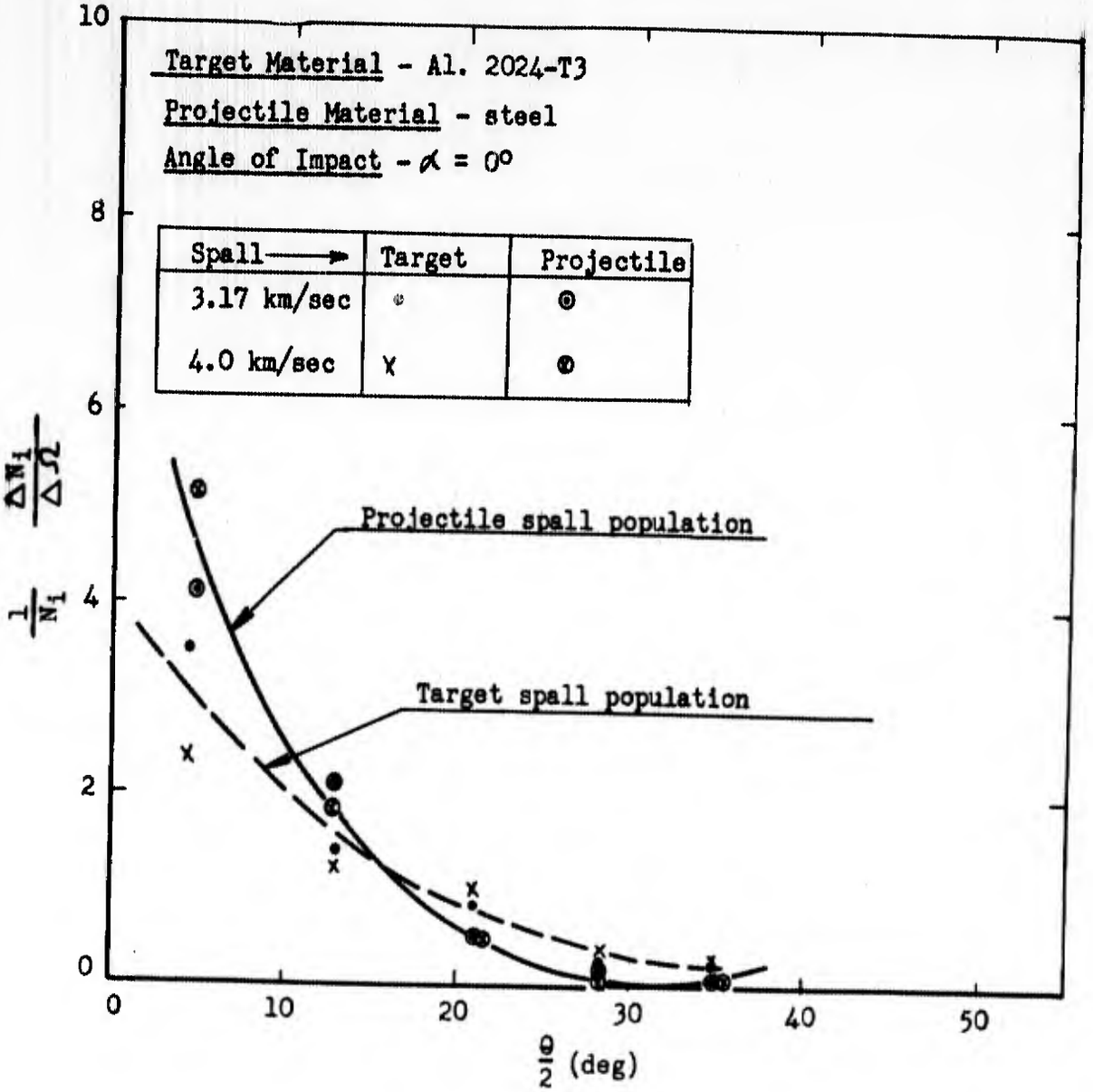

Fig. 6 Plot of normalized spall population distribution data separated into projectile spall and target spall as a function of $\theta/2$ for two projectile velocities.

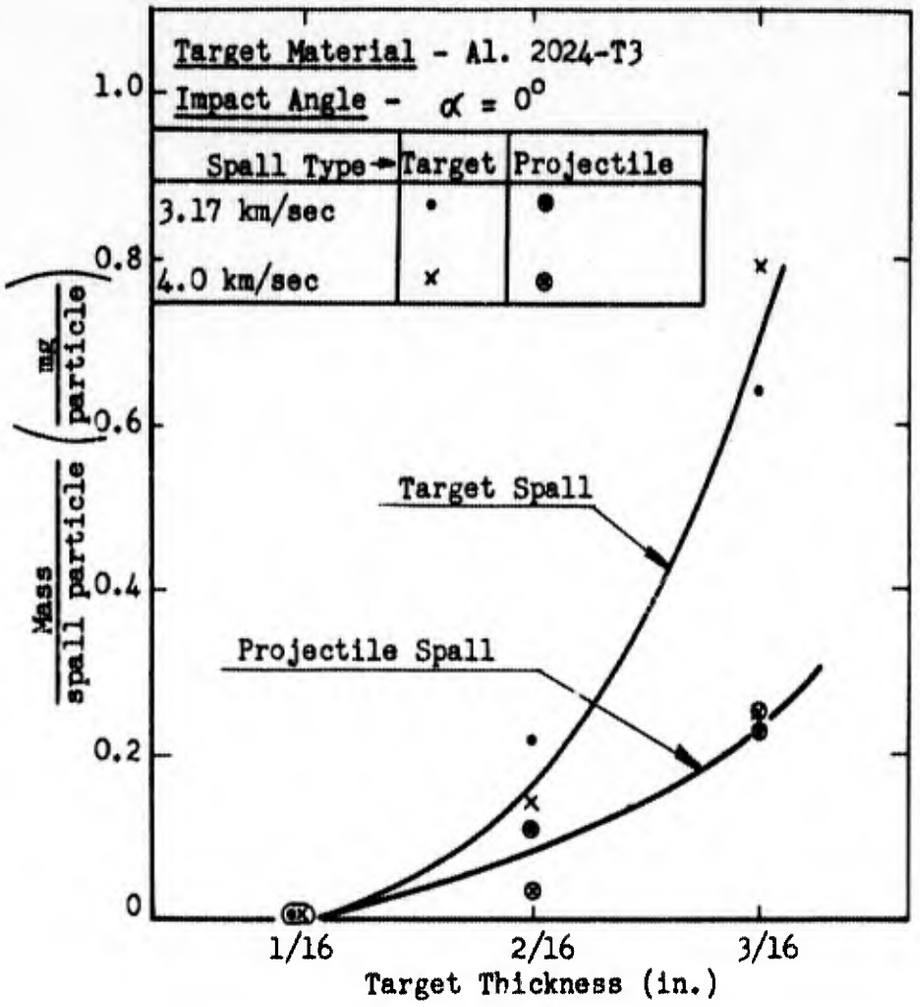

Fig. 7 Plot illustrating the average mass of a spall particle as a function of target thickness.

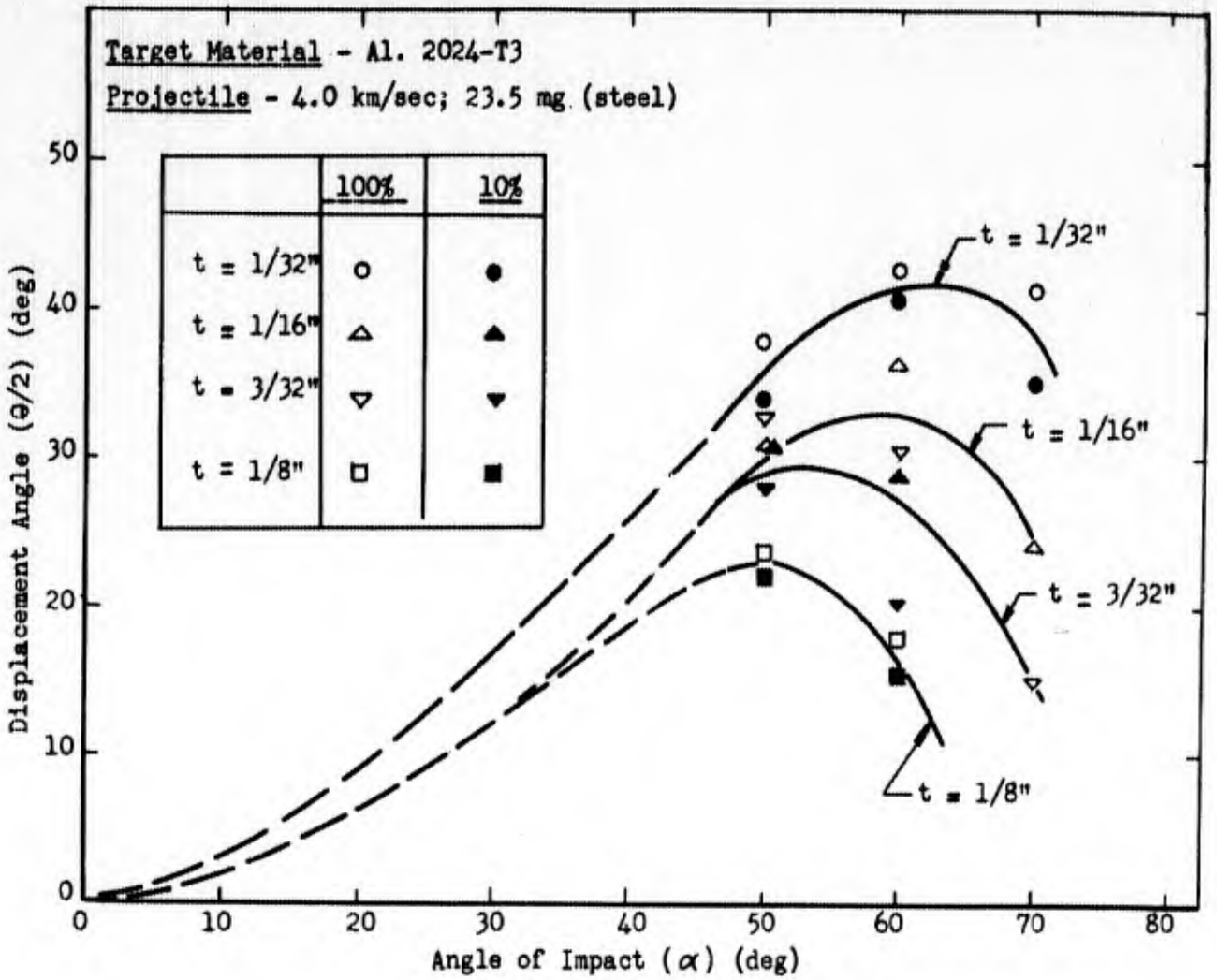

Fig. 8 Plot illustrating the displacement of the center of spall impact as a function of impact angle for several different target thicknesses. The plot shows data points for all spall fragments and for the 10 percent which have greater penetration capabilities.

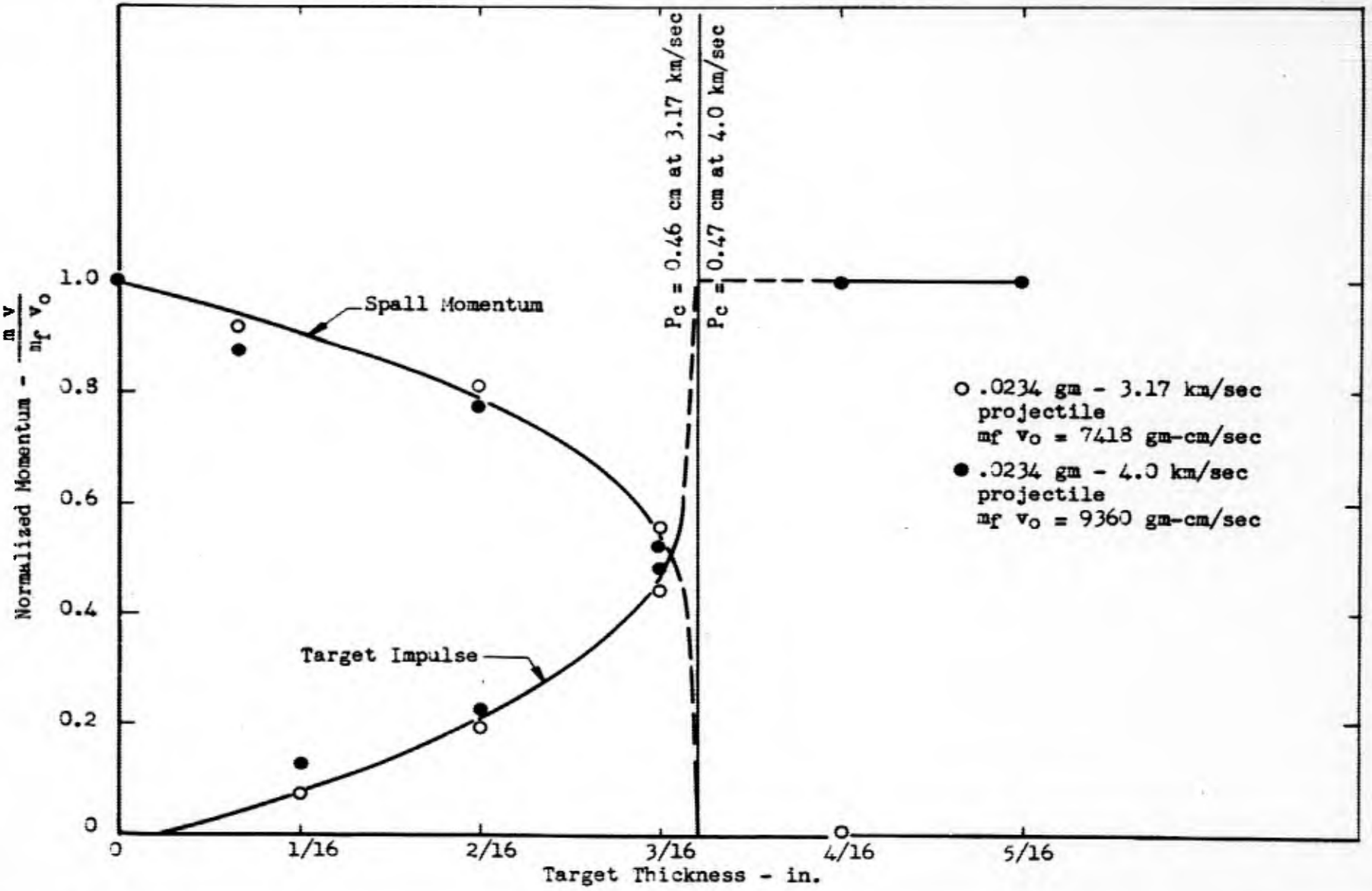

Fig. 9 Normalized target impulse and spall momentum as a function of target thickness for 2024-T3 aluminum targets impacted by .0234 gram steel projectiles having velocities of 3.17 km/sec and 4.0 km/sec.

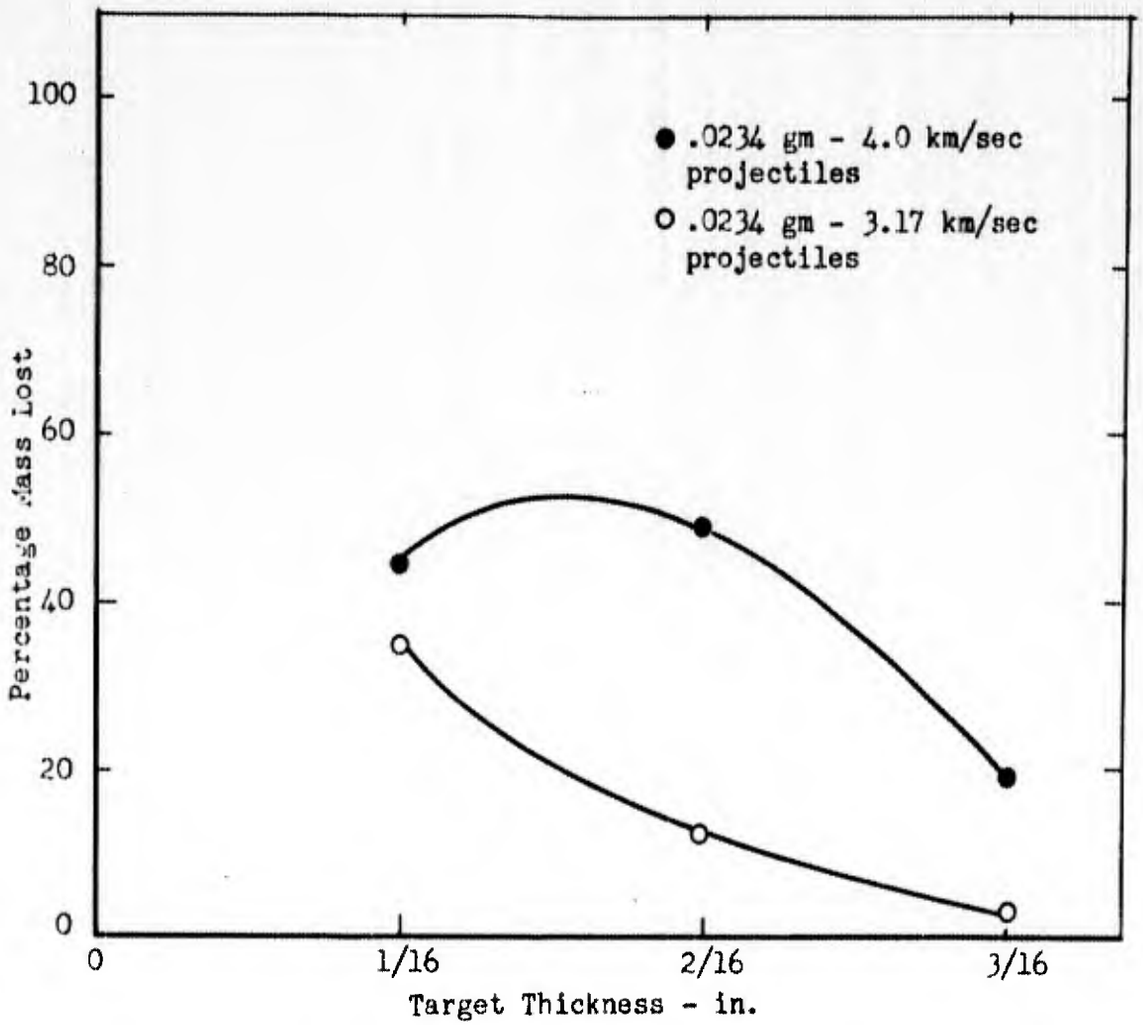

Fig. 10 Percentage of total target mass lost attributable to losses due to first surface effects for thin 2024-T3 Aluminum targets impacted at 3.17 and 4.0 km/sec.

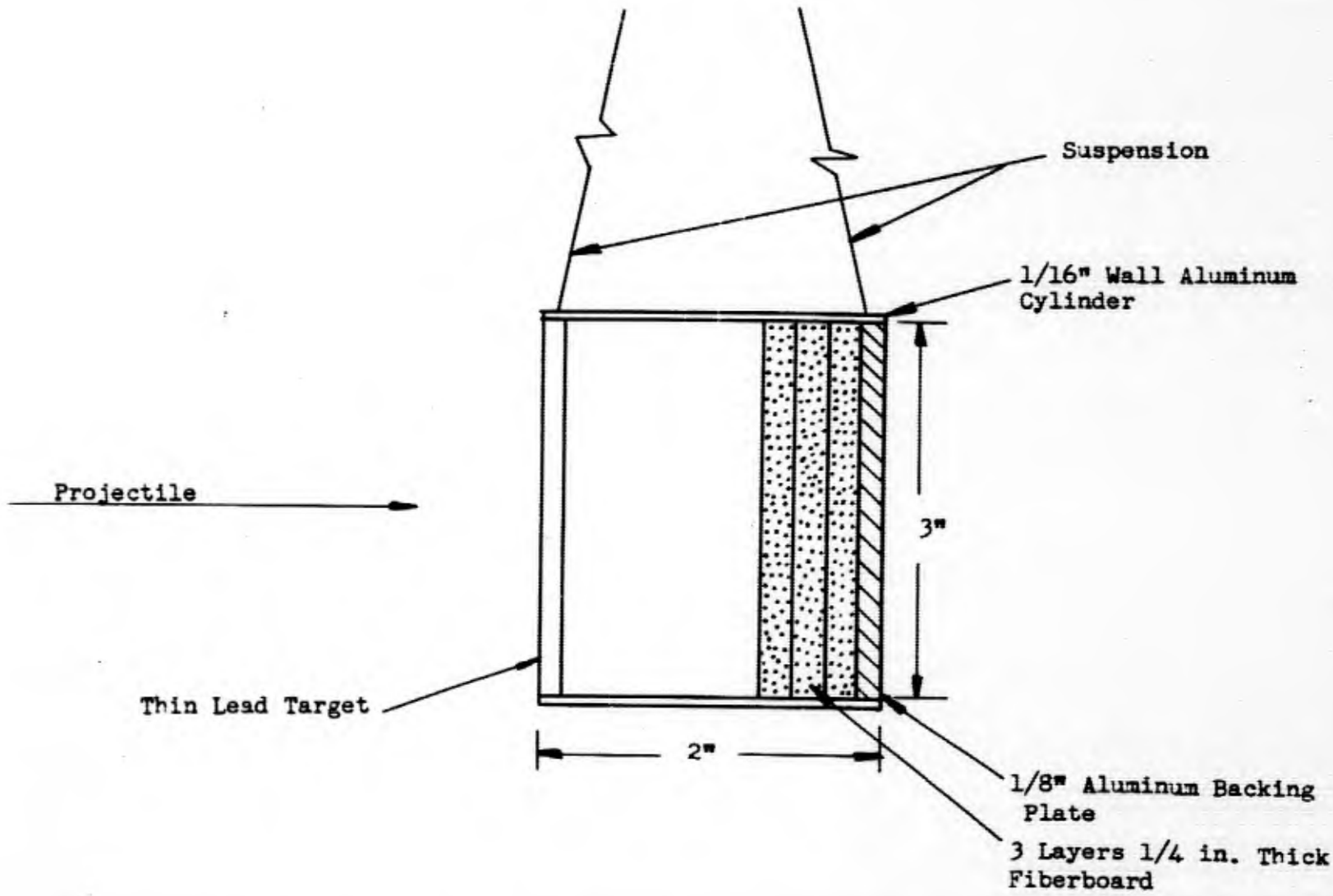

Fig. 11 Target arrangement used to total forward momentum impacted to lead target-spall system by the impact of .0234 gm steel cylinders with an initial velocities of 3.17 km/sec.

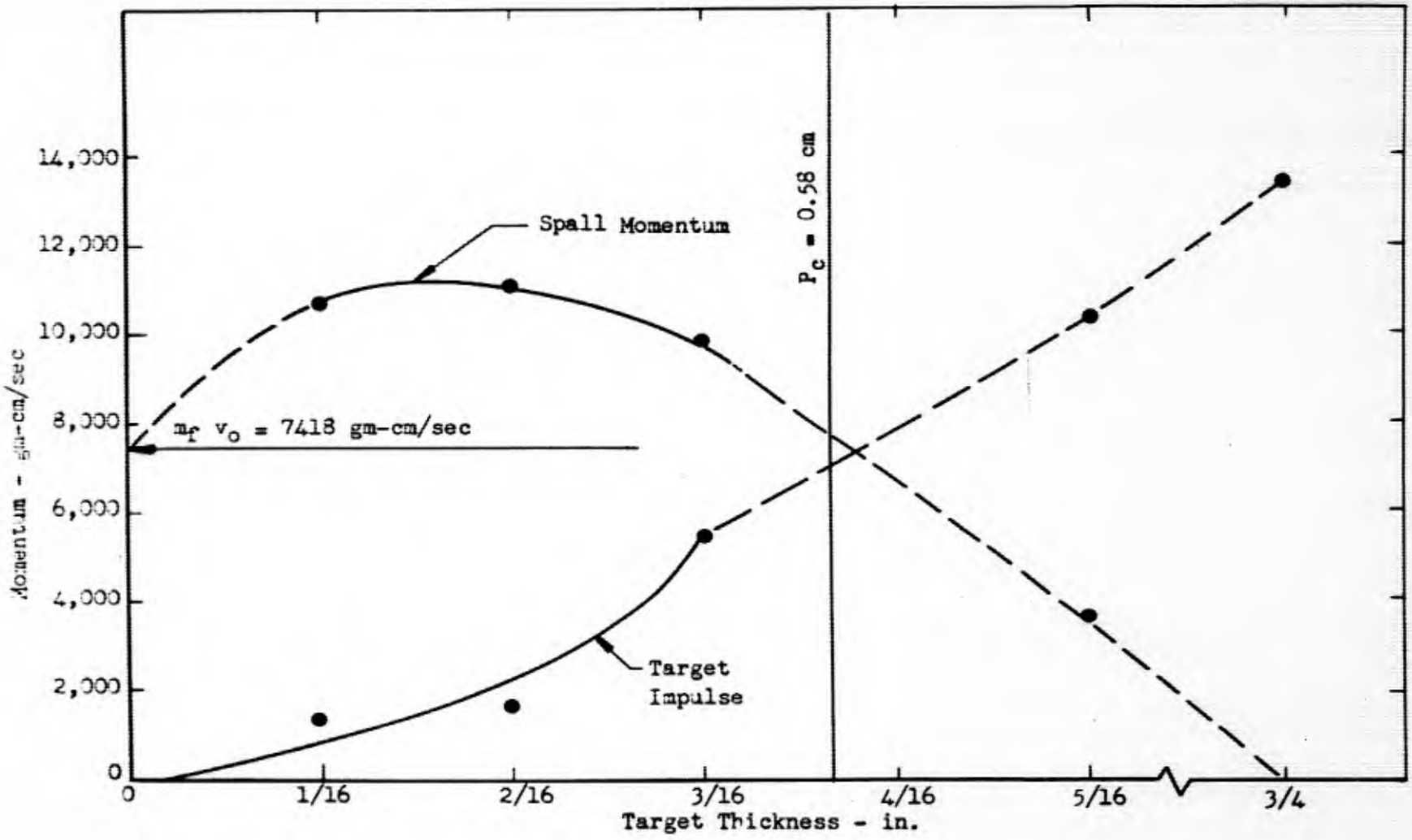

Fig. 12 Spall momentum and target impulse as a function of target thickness for lead targets impacted by .0234 gram projectiles having an initial velocity of 3.17 km/sec.

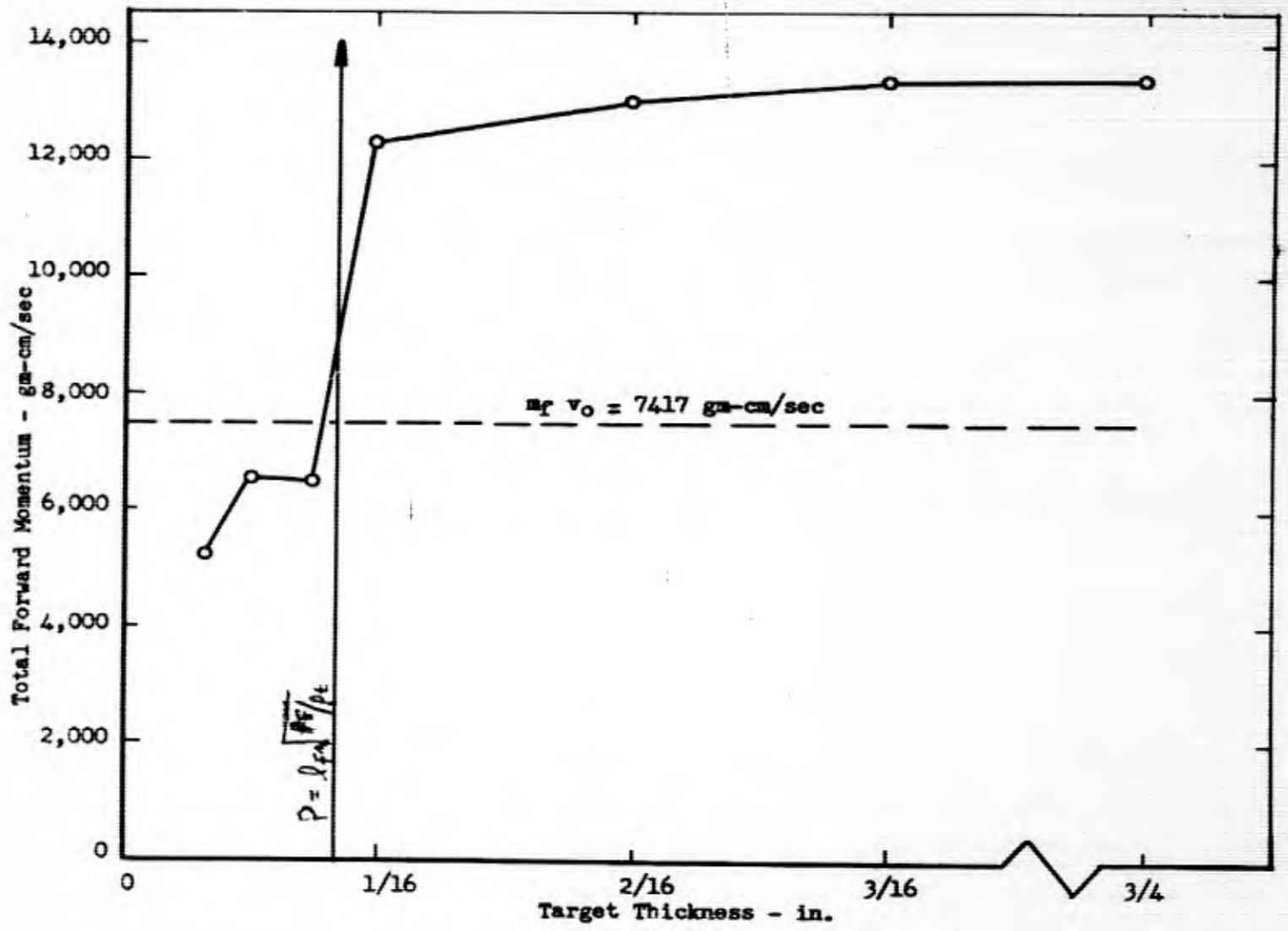

Fig. 13 Total forward momentum as a function of target thickness for lead targets impacted with 3.17 km/sec - .0234 gm steel projectiles. Note that the measured values of forward momentum are nearly constant for target thicknesses in excess of the depth of penetration predicted for this target-projectile combination on the basis of hydrodynamics.

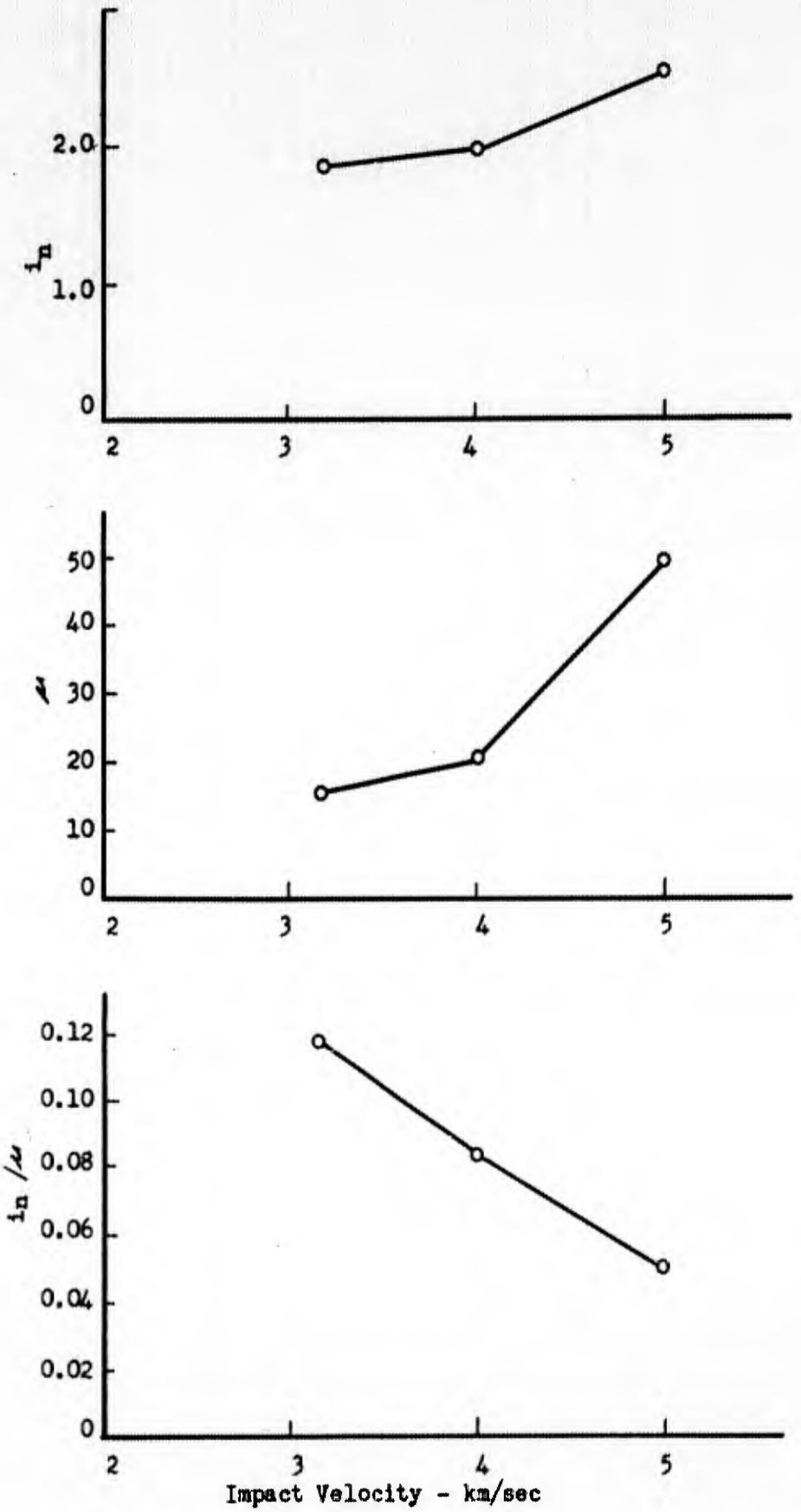

Fig. 14 Dependence of the momentum and mass parameters, i_n and μ, on impact velocity over the velocity range from 3.17 km/sec to 5.0 km/sec.

Table I. Tabulation of data associated with the mass distribution of spall (target spall and projectile spall) behind thin targets for 4.0 km/sec projectiles impacting aluminum 2024-T3 targets at normal incidence.

Solid Angle Ω	$\Delta\Omega$	Dispersion Angle (deg) ($\theta/2$)	Average Mass of Spall Fragments (mg) Target Thickness (in.) (1/16) ΔM	σ	(2/16) ΔM	σ	(3/16) ΔM	σ
0.074	.074	8.7	5.5 (74)	3.8	12.7 (172)	5.6	27.2 (367)	13.0
0.278	.204	17.1	8.7 (43)	3.9	30.5 (149)	4.5	65.1 (319)	19.3
0.578	.300	24.8	8.2 (27)	1.1	16.3 (54)	4.4	31.0 (103)	15.8
0.932	.354	31.6	5.4 (15)	1.1	17.2 (48)	2.6	20.0 (56)	1.9
1.303	.371	37.6	6.3 (17)	2.3	9.2 (25)	1.3	15.3 (41)	2.7
1.666	.363	42.7	3.4 (9)	0.9	7.3 (20)	3.4	17.0 (47)	11.7
Average Total Mass (mg)			37.5	1.9	93.2	8.8	175.6	14.1

Notes: (1) The masses given here include both projectile material and target material.

(2) Numbers in parentheses are $\Delta M/\Delta\Omega$. The $\Delta\Omega$ intervals are associated with Δr increments of 1.0 in. on a plane which is laid out in a family of concentric circles and is located 6.5 inches from the target plate. The solid angle (Ω) and dispersion angle ($\theta/2$) are specified at the end point of the interval.

(3) $\sigma = \text{range}/\sqrt{n}$; $(n = 3)$.

Table II. Tabulation of data associated with the mass distribution of projectile particles behind thin targets. The 4.0 km/sec projectiles impacted aluminum 2024-T3 targets at normal incidence.

Solid Angle Ω	$\Delta\Omega$	Dispersion Angle (deg) ($\theta/2$)	Average Mass of Projectile Particles (mg) Target Thickness (in.) (1/16) ΔM	σ	(2/16) ΔM	σ	(3/16) ΔM	σ
0.074	.074	8.7	2.3 (31)	0.7	3.1 (42)	2.8	5.0 (68)	1.7
0.278	.204	17.1	2.2 (11)	0.6	4.8 (24)	1.3	8.6 (42)	1.0
0.578	.300	24.8	0.7 (2)	0.6	1.4 (5)	1.5	1.3 (4)	0.6
0.932	.354	31.6	0.6 (2)	0.2	0.3 (1)	0.3	0.5 (1)	0.2
1.303	.371	37.6	0.3 (1)	0.1	0.3 (1)	0.1	0.3 (1)	0.1
1.666	.363	42.7	0.2 (1)	0.1	0.2 (1)	0.0	0.2 (1)	0.2
Average Total Mass (mg)			6.1	0.3	10.1	3.1	15.9	2.3

Notes: (1) The masses given here include only projectile (steel) masses as determined by chemical means.

(2) Numbers in parentheses are $\Delta M/\Delta\Omega$. The $\Delta\Omega$ intervals are associated with Δr (radial) increments of 1.0 in. on a plane which is laid out in a family of concentric circles and is located 6.5 inches from the target plate. The solid angle (Ω) and dispersion angle ($\theta/2$) are specified at the end point of the interval.

(3) σ = range/$\sqrt{n}$; (n = 3).

Table III. Tabulation of data associated with the breakdown of the population distribution of spall fragments into projectile fragments and target fragments.

$\theta/2$ (deg) (midpoint)	$\Delta\Omega$ (Sterad.)	v_o (km/sec)	ΔN_i 2/16 in. Targets Target Spall	2/16 in. Targets Projectile Spall	3/16 in. Targets Target Spall	3/16 in. Targets Projectile Spall
4.4	.074	3.17	62	82	40	14
		4.0	86	110	22	37
13.0	.204	3.17	119	79	22	37
		4.0	139	105	39	24
21.0	.300	3.17	67	10	40	22
		4.0	146	84	46	12
28.3	.354	3.17	29	8	13	11
		4.0	105	13	12	1
34.7	.371	3.17	20	4	10	4
		4.0	69	5	8	1
40.2	.363	3.17	3	1	1	1
		4.0	47	11	17	10
	$N_i \longrightarrow$	3.17	300	184	126	89
		4.0	592	328	144	85
	$N_i/N \times 100$	3.17	62%	38%	59%	41%
		4.0	64%	36%	62%	38%

Note: Targets were impacted at normal incidence; the target material was aluminum 2024-T3.

Table IV. Tabulation of data associated with centers of impact of spall patterns resulting from oblique impacts. The projectile velocity was 4.0 km/sec. and the target material was aluminum 2024-T3.

Impact Angle (α) (deg)	Target Thickness (in.)	N_i (1)	N_i (2)	(N_2/N_1 x 100)	Displacement Angle ($\theta/2$) (deg) (1)	Displacement Angle ($\theta/2$) (deg) (2)
50	1/32	634	67	10%	38.1	34.0
	1/16	889	110	12%	31.2	31.0
	3/32	715	69	10%	32.5	27.8
	1/8	284	17	6%	23.5	23.0
60	1/32	872	87	10%	42.5	40.5
	1/16	562	52	9%	36.4	27.9
	3/32	307	26	9%	30.0	20.0
	1/8	68	--	--	17.6	--
70	1/32	595	44	7%	42.2	34.7
	1/16	134	12	9%	24.2	--
	3/32	43	--	--	14.6	--

Note: (1) N_1 is the total number of spall fragments penetrating 1 mil of aluminum foil.

(2) N_2 is the total number of spall fragments penetrating an additional 7 mils of aluminum foil.

Table V. Results of target impulse studies made with 2024-T3 aluminum targets impacted at 4.0 km/sec.

Target Thickness (in.)	Total Forward* Momentum (gm-cm/sec)	Target Impulse (gm-cm/sec)	Normal Spall Momentum (gm-cm/sec)	Mass Lost (mg)	Mass Recovered (mg)
1/16	8,550	1,162	7,388	57.5	31.4
2/16	8,550	1,893	6,657	165.4	83.1
3/16	8,550	4,147	4,403	197.6	159.7
4/16	8,550	7,678	0	---	---
4/16 aluminum + 3/4 fiberboard	8,550	8,757	0	---	---
5/16	8,550	8,020	0	---	---
5/16 aluminum + 3/4 fiberboard	8,550	9,138	0	---	---
3/4	8,550	9,159	0	---	---

*Represents average of all measurements made in targets having thicknesses 1/4 inch or greater which represents the semi-infinite case.

Table VI. Measured values of total forward momentum and target impulse for various thicknesses of lead impacted with .0234 gm. steel projectiles having an initial velocity of 3.17 km/sec.

Target Thickness (in.)	Total Forward Momentum (gm-cm/sec)	Target Impulse (gm-cm/sec)	Normal Spall Momentum (gm-cm/sec)
.035	7,267	--	--
.049	7,558	--	--
1/16	12,073	1,211	10,862
2/16	12,982	1,484	11,498
3/16	13,346	3,633	9,713
4/16	--	--	--
5/16	--	10,500	2,850
3/4	13,350	13,350	0

Table VII. Total impulse and mass loss data for "semi-infinite" lead targets impacted with steel projectiles having initial velocities of 3.17 km/sec., 4.0 km/sec., and 5.0 km/sec.

Impact Velocity (km/sec)	Projectile Mass (gm)	Target Impulse (gm-cm/sec)	Target Mass Loss (gm)	i_n*	Δ**
3.17	.0234	13,350	.358	1.8	15.2
4.0	.0234	16,358	.477	1.91	20.4
5.0	.18	232,378	8.9	2.58	49.5

*The parameter, i_n, is the ratio of target impulse to the momentum of the impacting fragment.

**The parameter, Δ, is the ratio of target mass lost to the mass of the impacting fragment.

DISTRIBUTION LIST FOR

Type I Quarterly Report

on

Hypervelocity Impact Phenomena

Sponsored by the Department of the Army
Aberdeen Proving Ground

Commanding General
Aberdeen Proving Ground
Maryland
Attn: R. J. Eichelberger
Ballistic Research Laboratories

Commanding General
Aberdeen Proving Ground
Maryland
Attn: J. Kineke
Ballistic Research Laboratories

Commanding General
Aberdeen Proving Ground
Maryland
Attn: Technical Library
Ballistic Research Laboratories

Office, Chief of Ordnance
Department of the Army
Washington 25, D. C.
Attn: ORDTU

British Joint Services Mission
1800 K Street, N. W.
Washington 6, D. C.
Attn: Reports Officer

Commanding Officer
U. S. Naval Ordnance Test Station
China Lake, California
Attn: J. W. Rogers

Commanding Officer
Air Proving Ground Center
Eglin Air Force Base, Florida
Attn: H. L. Davis

Commanding General
Aberdeen Proving Ground
Maryland
Attn: S. Kronman
Ballistic Research Laboratories

Commanding General
Aberdeen Proving Ground
Maryland
Attn: F. E. Allison
Ballistic Research Laboratories

Office, Chief of Ordnance
Department of the Army
Washington 25, D. C.
Attn: ORDTB, Ballistics Section
Mr. M. C. Miller

Commanding Officer
Armed Services Technical Information
Agency
Arlington Hall Station
Arlington 12, Virginia
Attn: TIPCR

Canadian Army Staff
2450 Massachusetts Avenue
Washington 8, D. C.

Director
U. S. Naval Research Laboratory
Washington 25, D. C.
Attn: Mr. W. W. Atkins, Code 130

Commanding Officer
Air Proving Ground Center
Eglin Air Force Base, Florida
Attn: Lt. W. H. Dittrich
Det. 4, ASD(ASQWR)

Director, The RAND Corporation
1700 Main Street
Santa Monica, California
Attn: J. H. Huth

Director, The RAND Corporation
1700 Main Street
Santa Monica, California
Attn: R. L. Bjork

Director, The RAND Corporation
1700 Main Street
Santa Monica, California
Attn: Technical Library

Library of Congress
Technical Information Division
Reference Department
Washington 25, D. C.
Attn: Bibliograph Section

General Motors Corporation
Defense Systems Div., Box T
Santa Barbara, California
Attn: J. W. Gehring

Firestone Tire & Rubber Company
1200 Firestone Parkway
Akron, Ohio
Attn: C. M. Cox

Commanding Officer
Air Proving Ground Center
Eglin Air Force Base, Florida
Attn: F. E. Howard
Det. 4, ASD(ASQP)

Director, National Aeronautics &
Space Administration
Ames Research Center
Moffett Field, California
Attn: J. L. Summers

Director, National Aeronautics &
Space Administration
Ames Research Center
Moffett Field, California
Attn: Technical Library

Director, National Aeronautics &
Space Administration
Langley Research Center
Langley Field, Virginia
Attn: W. H. Kinard

Director, National Aeronautics &
Space Administration
Langley Research Center
Langley Field, Virginia
Attn: Technical Library

General Motors Corporation
Defense Systems Div., Box T
Santa Barbara, California
Attn: Technical Library

Aeroelastic & Structures Laboratory
Massachusetts Institute of Technology
77 Massachusetts Avenue
Cambridge 39, Massachusetts
Attn: W. Herrmann

Drexel Institute of Technology
Mechanical Engineering Dept.
Philadelphia 4, Pennsylvania
Attn: Pei Chi Chou

Int.-Burlines, Pittsburgh, Pa.